Journal of Analytical and Applied Pyrolysis 185 (2025) 106873

Contents lists available at ScienceDirect

Journal of Analytical and Applied Pyrolysis

journal homepage: www.elsevier.com/locate/jaap

Comprehensive study on co-pyrolysis mechanisms of sewage sludge and low rank coal under rapid/slow heating conditions

Chenyang Liu [a,b], Zhongjie Shen [a,b,*], Haigang Zhang [a,b], Guinan He [a,b], Weifeng Li [a,b], Haifeng Liu [a,b,c]

[a] National Energy Coal Gasification Technology Research and Development Center, East China University of Science and Technology, P. O. Box 272, Shanghai 200237, PR China
[b] Shanghai Engineering Research Center of Coal Gasification, East China University of Science and Technology, P. O. Box 272, Shanghai 200237, PR China
[c] Liaoning Petrochemical University, Fushun, Liaoning 113001, PR China

ARTICLE INFO

Keywords:
Sewage sludge
Low rank coal
Rapid/slow co-pyrolysis
Gas release rule
Synergistic effect

ABSTRACT

Co-pyrolysis of sewage sludge (SS) and low rank bituminous coal (BC) was considered as an effective technology in realising the co-resource utilization and disposal of municipal waste. The current work focused on the co-pyrolysis characteristics and synergistic mechanisms under rapid/slow heating conditions, with experimental and analytical methods of the thermogravimetric-mass spectrometry (TG-MS), gas chromatography (GC), and Fourier transform infrared spectroscopy (FTIR). The results showed that the heating rate and mixing ratio of SS and BC caused different yields of the co-pyrolysis products. The gas products performed different releasing rules with the effect of mixing ratio of SS and BC, and the different stages during the slow pyrolysis were defined in terms of weight loss and product release. Under the rapid heating condition, the gas product yield in the experiment was found to be consistently higher than the theoretical yield, regardless of the mixing ratio. The addition of SS in the mixtures would increase the yield content of CO_2 and high calorific gases (C_2H_2, C_2H_4, C_2H_6) and reduce H_2, CO, and CH_4. The intensities and widths of the absorption peaks of functional groups such as O-H, C-H, C=O and C=C in the char decreased. The morphology, pore structure, and particle size distribution of the pyrolyzed samples were compared and analysed. Kinetic analysis was carried out according to different stages of slow pyrolysis. Finally, the synergistic effect and mechanism of the co-pyrolysis were comprehensively compared and revealed under slow/rapid heating conditions.

1. Introduction

The extensive utilization of fossil energy has contributed to the rapid development of the global economy, while the CO_2 emission issue from the fossil fuel consumption was becoming an urgent issue. With a growing global emphasis on the sustainable development and ecological maintain, it was imperative to seek out clean renewable energy sources and green processes [1]. Sewage sludge, as an essential by-product of conventional wastewater treatment, has inevitably increased rapidly during the process of urbanisation and industrialisation [2]. The improper disposal of sewage sludge would cause secondary pollution to water sources, soil and even public health [3]. The conventional disposal methods included landfill, agricultural application, and thermochemical conversion to fuels [4]. Among these, incineration has been widely used in the past but required deep drying and dehumidification to maintain the combustion stability, which was costly, especially in developing countries [5]. Pyrolysis, as a low energy consuming and environmentally friendly process has been received extensive attention. The pyrolysis of sewage sludge could produce gas, solid, and liquid fuels, and the product properties have significant impacts on the subsequent combustion, gasification and liquefaction processes [6].

Sewage sludge was composed of diverse solid particles suspended in an impure water continuum, with a very high ratio of water to solids, relatively homogeneous and pumpable, and exhibited rheological properties of a "Bingham plastic" [7]. Sewage sludge contained complex organic (proteins, carbohydrates, fats and oil) and inorganic (metals) compounds, and a wide variety of living and dead microorganisms [8]. The pyrolysis behaviour of the main components of the sewage sludge

* Corresponding author at: National Energy Coal Gasification Technology Research and Development Center, East China University of Science and Technology, P. O. Box 272, Shanghai 200237, PR China.
E-mail address: zjshen@ecust.edu.cn (Z. Shen).

https://doi.org/10.1016/j.jaap.2024.106873
Received 27 September 2024; Received in revised form 16 November 2024; Accepted 19 November 2024
Available online 22 November 2024

Table 1
Proximate and ultimate analyses and heating value of BC, SS, and blends with different ratios.

Material	Proximate analysis(wt%, ad[a])				Ultimate analysis(wt%, ad)					Q_b[c](MJ/kg)
	M	A	V	FC	C	H	O[b]	N	S	
BC	2.16	7.74	30.68	59.42	76.61	3.66	8.37	0.90	0.56	28.421
BC7-SS3	4.08	17.92	34.56	43.44	62.53	3.86	8.78	1.99	0.84	22.483
BC5-SS5	5.56	24.33	37.28	32.83	52.07	3.97	10.49	2.68	0.90	19.077
BC3-SS7	7.02	30.77	40.53	21.68	42.77	4.07	10.98	3.36	1.03	15.547
SS	9.17	40.34	46.13	4.36	26.49	4.19	14.15	4.53	1.13	10.195

[a] Air dried
[b] O (oxygen) was calculated by difference
[c] Bomb calorific value.

was comparable to the coal or biomass resources, and it could be regarded as a special bioenergy, classified to a type of biomass [9]. In the dry form, sewage sludge could also be considered a special type of renewable fuel [10]. Owing to the low heating value of sewage sludge, the disposal process was added other fuels of relatively-high heating value, such as low rank coal, to improve the respective pyrolysis characteristics [11]. Sewage sludge and low rank coal as biomass fuels have already accounted for about 10 % of the global non-conventional renewable energy supply [12]. Therefore, the knowledge of the co-pyrolysis of sewage sludge and low rank coal could help to convert organic matters in the sewage sludge to potential high value fuels.

The study uncovered that during the co-pyrolysis of coal and petrochemical wastewater sludge in the packed-bed reactor, the yields of solid char and liquid were lower than the theoretically calculated values, suggesting that the synergistic effects significantly contributed to the release of gas products [13]. Moreover, co-pyrolysis of coal and dry sludge also exhibited significant synergistic effects on the removal of N and S [14]. In particular, the release of sulphur-containing pollutants, such as H_2S and SO_2, was significantly inhibited, and the inhibition effect was pronounced when the mixing ratio of sludge to coal was 50:50 [15]. If co-pyrolysis of fly ash and oily sludge was used at the same mixing ratio, the maximum yields of pyrolysis oil and gas could be increased by 13.85 % and 2.24 %, respectively [16]. In addition, according to the Vyazovkin model calculations, the incorporation of 10 % of paper sludge in coal pyrolysis was able to increase the pyrolysis reactivity of coal [17]. At the same mixing ratio, the activation energy of the blend was lower than the theoretically calculated value [18]. This effect was even more significant if 5 % MgO or 5 % AC (activated carbon) was also added as a catalyst for the co-pyrolysis [19]. Although the co-pyrolysis of sewage sludge and low rank coal with various solid fuels has been studied and reported in the literature, there were few studies on the thermochemical properties, product distribution, and gas product release rule of the co-pyrolysis under the rapid/slow heating condition, and the synergistic effects that exist were ambiguous and still need to be further explored.

The comparative study on the rapid/slow co-pyrolysis characteristics of SS and BC was conducted with multiple experimental and analytical methods. The weight loss and rate, gas product composition, and solid sample of the mixture sample of SS and BC were analysed and compared. The evolution in functional groups, surface morphology, specific surface area and porosity of the char samples after co-pyrolysis were characterised, and the release characteristics and formation mechanisms of co-pyrolysis gases were analysed. The synergistic effects and mechanisms of SS and BC mixtures under rapid/slow heating conditions were comprehensively proposed, based on the physicochemical properties and kinetic analyses of the gas and solid products, providing a potential support for the practical application of sewage sludge and low rank coal in co-thermal conversion.

2. Material and method

2.1. Materials

The sewage sludge sample was a municipal sewage sludge (SS), and the coal sample used in this study was a low rank bituminous coal (BC) from Xinjiang, China. The SS and BC samples were dried at 105 °C for 12 h, then pulverized and sieved through 100 mesh (150 μm) and 200 mesh (75 μm) screens to separate experimental samples with particle sizes less than 150 μm. The BC and SS mixtures were homogeneously mixed in mass ratios of 10:0, 7:3, 5:5, 3:7, and 0:10 to prepare five blends, designated as BC, BC7-SS3, BC5-SS5, BC3-SS7, and SS. The proximate and ultimate analyses and calorific value of BC and SS were measured, and the results were shown at Table 1. The proximate analysis data was tested by a fully automatic proximate analyser (Changsha Kaiyuan Instruments, 5E-MACIII and 5E-MVC6700, China). The ultimate analysis data was tested by an elemental analyser (Elementar, vario MACRO CUBE, Germany), and the heating value was tested by an isothermal fully automatic calorimeter (Changsha Kaiyuan Instruments,

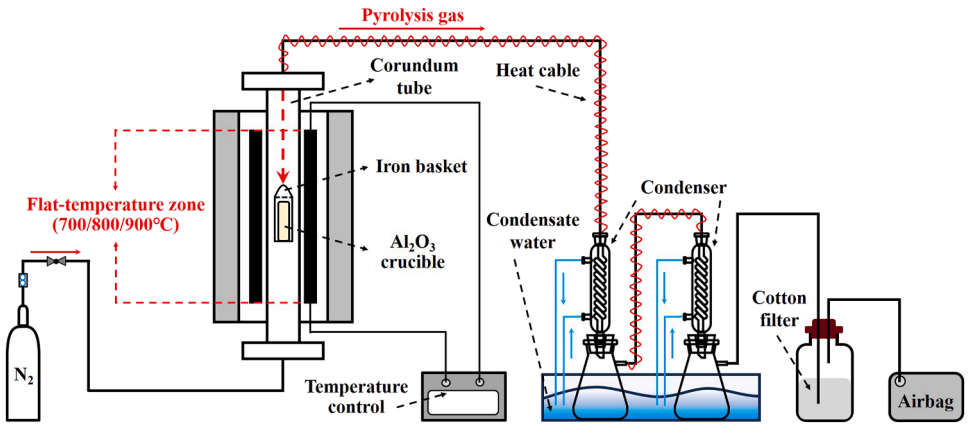

Fig. 1. Schematic diagram of the tube furnace reactor used in this study.

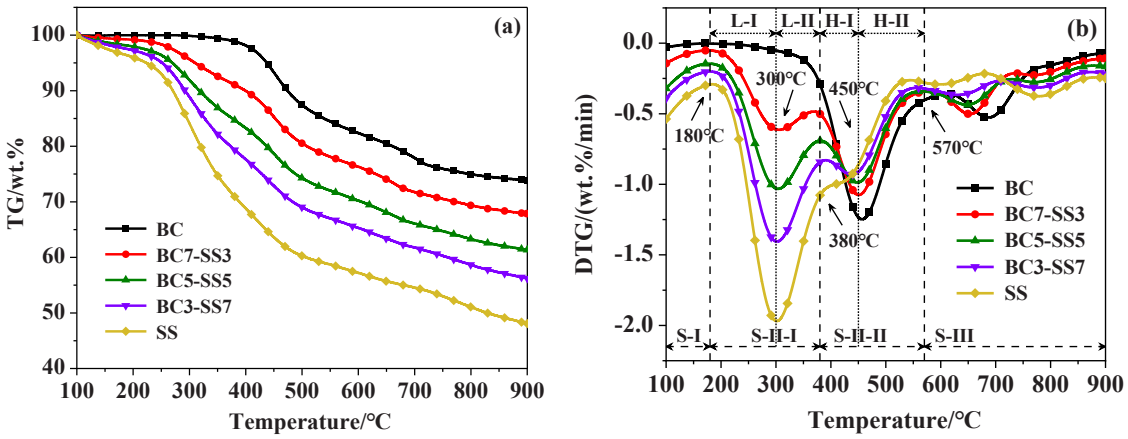

Fig. 2. Thermogravimetric (TG) and weight loss rate (DTG) curves of BC, SS, and blends at 10 °C/min: (a) TG, (b) DTG.

5E-AC8018, China).

2.2. Experimental and analytical methods

The non-isothermal slow co-pyrolysis of BC and SS samples were performed in the TG-MS (NETZSCH, STA 449 F3 Jupiter-QMS 403 D Aëolos, Germany). 10 mg of sample was loaded and heated from 30 to 900 ℃. The heating rate and N_2 (purity 99.999 %) flow rate were fixed at 10 ℃/min and 100 mL/min, respectively. The loss of sample weight and the rate were continuously recorded, and to ensure the accuracy and least error, experiment was repeated at least three times.

To investigate isothermal rapid co-pyrolysis characteristics of BC and SS mixtures, a laboratory-scale tube furnace reactor (TFR, Shanghai Yuzhi Technology, China) was used as shown in Fig. 1. Before the start of experiment, the TFR was preheated from 50 °C to the setting temperature (700 ℃, 800 ℃, or 900 ℃) at a heating rate of 10 ℃/min, and introduced N_2 with a flow rate of 100 mL/min throughout the process to remove the air inside the TFR to ensure an inert atmosphere. A sample of 10 g was placed into the Al_2O_3 crucible and then positioned the crucible into a high temperature resistant (<1200 °C) hanging basket made of 310S austenitic chromium-nickel stainless steel. Once the TFR reached the set temperature, the basket was quickly placed to the thermostatic reaction area and the rapid co-pyrolysis reaction was carried out for 10 min under N_2 with a flow rate of 100 mL/min. The co-pyrolysis gases were passed through two consecutive condensers and then the non-condensable gases were collected in the gas bag. After 10 min, the sample was quickly moved to cold side of the TFR, and then cooled down to room temperature under N_2 atmosphere before collecting the chars. Simultaneously, N_2 with a flow rate of 1000 mL/min was used to purge the TFR for 20 min and the gas bag were replaced to collect the remaining reaction gases, ensuring that the reaction gases generated from the previous sample was completely collected before proceeding to the next experiment. The mass of liquid products dissolved from the condenser was determined using C_4H_8O (Macklin, AR, purity 99.0 %), and the heat cables were wrapped around the gas pipelines to make sure the volatile matter was completely trapped in the condensers. At least three repeat runs were conducted under the same conditions to ensure the repeatability of the experiment.

The gas products were analysed by the gas chromatography (Agilent, 990 Micro GC, America) with the thermal conductivity detector (TCD). The char was analysed for functional group evolution by the Fourier transform infrared spectroscopy (Thermo Scientific, NICOLET iS50 FT-IR, America), the surface morphology of char was characterized by the scanning electron microscopy (HITACHI, SUI5IO, Japan), the porosity and particle size evolution of the char was characterized by the surface area and pore size analyser (Micromeritics, ASAP 2460 and VacPrep 061, America) and the laser particle size analyser (Malvern Instruments, Mastersizer 2000, Britain).

To evaluate whether the synergistic effects existed between the BC and SS mixtures, the theoretical yields of the pyrolysis products of the blends were calculated and compared with the experimental yields. The theoretical yields of char, gas and liquid products were adopted to the weighted average method by following Eq. (1) [20]:

$$Y_{Cal} = X_{BC} \times Y_{BC} + X_{SS} \times Y_{SS} \quad (1)$$

where Y_{Cal} is the calculation yield (%); X_{BC} and X_{SS} are the mass percentage (wt%) of BC and SS in the blend, respectively; Y_{BC} and Y_{SS} are the experimental yield (%) of BC and SS, respectively; the experimental yield can be calculated as Eqs. (2–4) [21]:

$$Y_{Char} = \frac{W_{Char}}{W_{raw}} \times 100\% \quad (2)$$

$$Y_{Gas} = \frac{W_{Gas}}{W_{raw}} \times 100\% \quad (3)$$

$$Y_{Liquid} = 1 - Y_{Char} - Y_{Gas} \quad (4)$$

where Y_{Char} , Y_{Gas} , Y_{Liquid} are the yield (%) of char, gas, liquid, respectively; W_{raw} is the mass (g) of raw material; W_{Char} is the mass (g) of char, which is obtained by direct weighing; W_{Gas} is the mass (g) of gas, which is calculated by quantifying the N_2 flow rate as Eq. (5):

$$W_{Gas} = \sum_i \frac{V_{N_2} \times v_i \times M_i}{v_{N_2} \times V_m} \quad (5)$$

where i corresponds to H_2, CH_4, CO, CO_2, C_2H_2, C_2H_4, C_2H_6 of main gas component, respectively; V_{N_2} is the total volume (L) of N_2 supplied; v_i is the percentage of each gas volume (%).

3. Result and discussion

3.1. Slow co-pyrolysis characteristics

Fig. 2 presented the TG and DTG curves of the pyrolysis of BC, SS, and their mixtures at different mixing ratios. Fig. 2(a) showed that the weights of all the tested samples were reducing when the temperature increased from 100 to 900 ℃, and the final weigh loss was different from samples. According to the data in Fig. 2(a), the weight loss rate (DTG) was calculated and shown in Fig. 2(b). The pyrolysis process was divided into three distinct stages depending on the amount of weight loss rate during the reaction in Fig. 2(a): Stage S-I (≤180 °C), Stage S-II (180–570 ℃), and Stage S-III (≥570 ℃). Within the S-I stage, both BC and SS samples underwent dehydration reaction. At Stage S-II, the peak weight loss rate of BC sample was observed at 457 °C, with the maximum

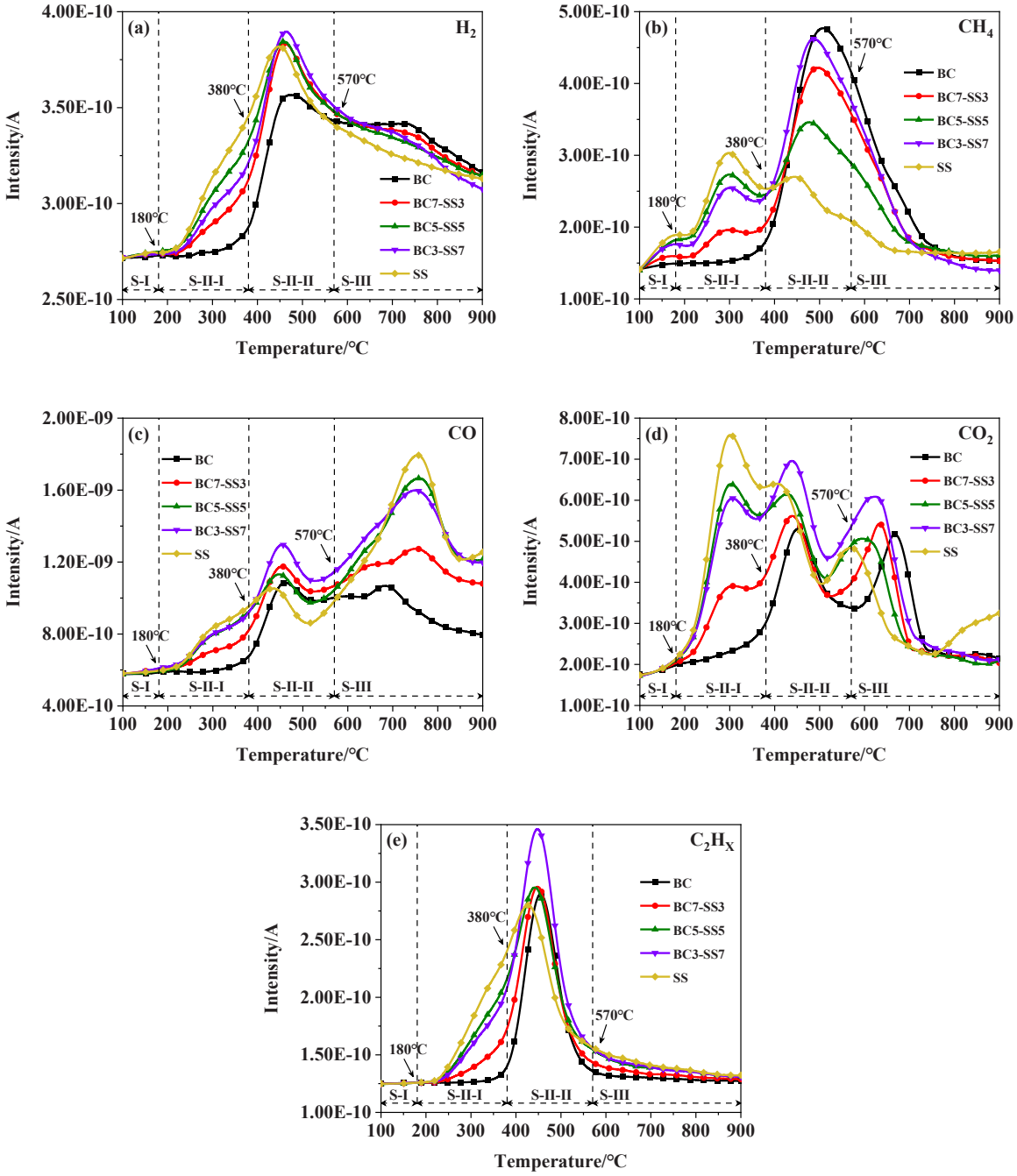

Fig. 3. The mass spectrometry (MS) analysis curves of BC, SS, and blends at 10 °C/min: (a) H_2, (b) CH_4, (c) CO, (d) CO_2, and (e) C_2H_x(x=2, 4, 6).

weight loss rate being 1.25 wt%/min. The maximum weight loss rate of the SS sample was 1.97 wt%/min, which corresponded to the peak at 301 °C, and the shoulder peak near 425 °C was associated with the one-step degradation of intermediate products derived from the lipids and proteins [22]. In the S-III stage, a peak was observed for both BC and SS samples.

Within the aforementioned three temperature stages, the co-pyrolysis processes of the BC and SS mixtures exhibited three distinct peaks. The peak intensity of the blend sample at 300 ℃ gradually transformed while the peak at 450 ℃ displayed an increasing tendency, with the decrease of the SS in the blends. Thus, the S-II stage (180–570 ℃) could be further divided into two sub-stages: S-II-I (180–380 ℃) and S-II-II (380–570 ℃). At Stage S-III, the peak for BC sample was attributed to the secondary cracking of high molecular weight liquid [23], while for the SS sample, it was due to the decomposition of minerals such as calcium carbonate and the gasification of the chars [24]. S-II-I and S-II-II were divided into four temperature stages (L-I (453–573 K), L-II (573–653 K), H-I (653–723 K) and H-II (723–843 K) for kinetic analysis in the Section 3.5.

The gas release curves and components from the mass spectrometry (MS) analysis of BC, SS and blends are shown in Fig. 3. Compared to the weight loss in the Stage S-II-I, from Fig. 3(b) and (d), the primary reactions included degasification and decarboxylation. CO_2, CH_4, and N_2, which were adsorbed and enclosed within the pores of BC and SS, were released and part of labile functional groups such as carboxyl groups cracked to generate CO_2 and H_2O. In this stage, the maximum weight loss rate of BC7-SS3, BC5-SS5 and BC3-SS7 were 0.61 wt%/min, 1.03 wt%/min and 1.41 wt%/min, respectively. Meanwhile, the difference in weight loss rate in Fig. 2 was the maximum value of the entire pyrolysis process, and the temperature of the peaks of the blends and SS

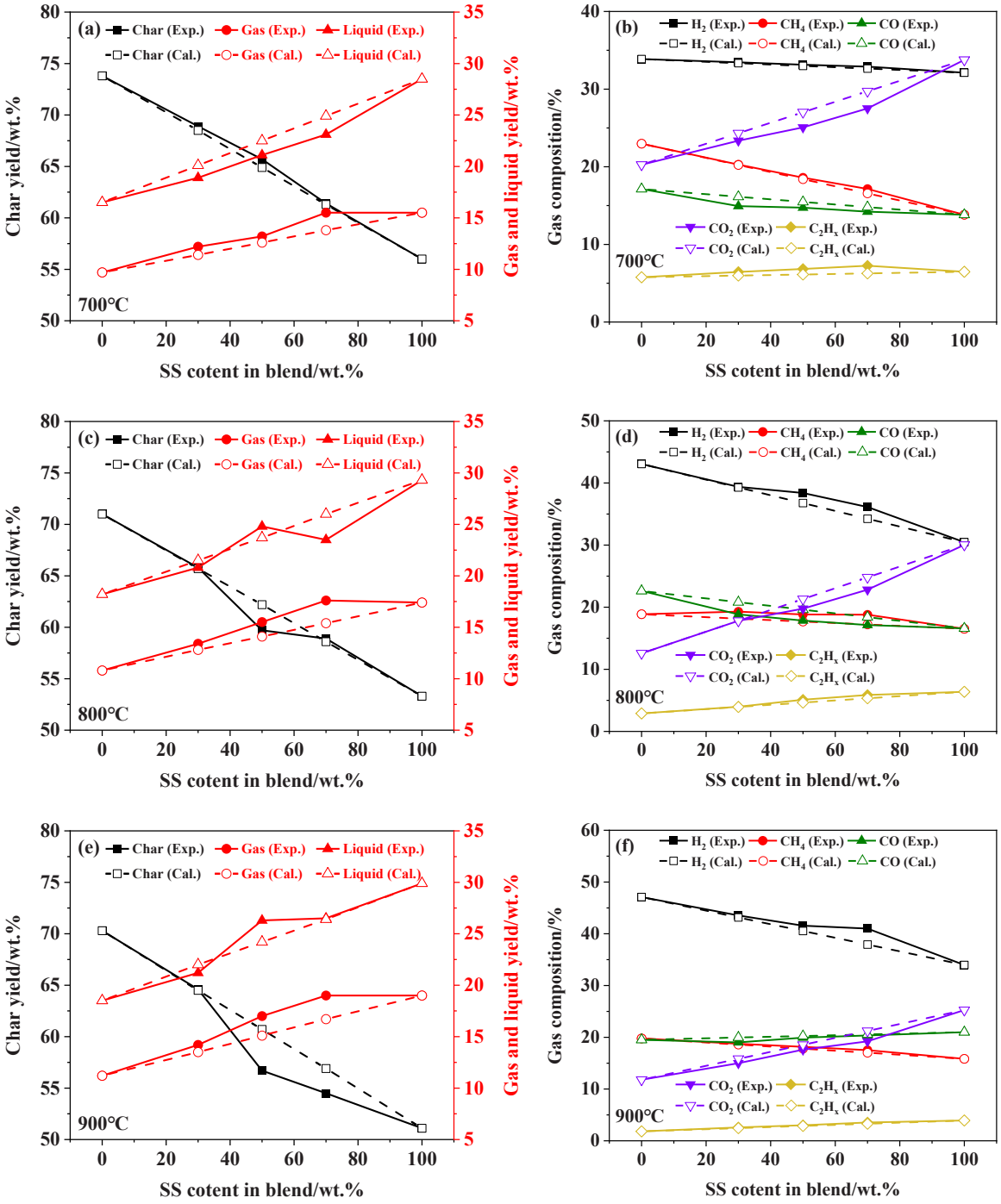

Fig. 4. Experimental and calculated yields of co-pyrolysis products and gas composition of BC, SS, and blends under rapid heating conditions: (a-b) 700 ℃, (c-d) 800 ℃, and (e-f) 900 ℃.

corresponded to each other. This indicated that the weight loss of the blends at lower temperatures was primarily attributed to the pyrolysis of SS. From Fig. 3(a) and (e), in stage S-II-II, the primary reactions were depolymerization and decomposition, where the volatile components consisting of H_2, CO, CO_2, H_2O and high calorific value gases (CH_4, C_2H_2, C_2H_4, C_2H_6) were successively decomposed. At higher temperatures, the pyrolysis of BC component in the blends was intensified, and the peaks of the blends and BC were corresponded to each other. Stage S-III involved the thermal condensation and carbonization reactions, where the low peak observed of the blends was attributed not only to the continued decomposition of semi-coke into char with the concurrent release of a substantial amount of H_2, but to the further cracking of C-C and C-H bonds. As illustrated in Fig. 3, the precipitation peaks of gaseous products of the BC3-SS7 were significantly higher than other blends, particularly in high calorific value gases, which was attributed to the decomposition of SS and release of volatile matter at lower temperatures.

3.2. *Rapid co-pyrolysis products*

Fig. 4 gives the experimental and calculated yields of co-pyrolysis products and gas compositions of BC, SS and blends at rapid heating conditions of different temperatures. In Fig. 4(a), (c) and (e), according to the calculation of Eqs. (2–5), the char yield was negatively correlated

with the increase of SS mixing ratio or pyrolysis temperature, while the pyrolysis gas and liquid yields were positively correlated. This was due to the high fixed carbon content in BC, thus the solid char being the main pyrolysis product. Whereas, the SS, with the higher volatile content, had more condensable gas and liquid products. According to Eq. (1), the experimental yields of the gas products were consistently higher than the theoretical yields at different temperatures. The yields of BC3-SS7 had the significant difference and increased with the temperature, which were 1.70 % at 700 °C, 2.20 % at 800 °C, and 2.30 % at 900 °C, respectively. The experimental yield of char at 700 °C was essentially in line with the theoretical value, and the increase of pyrolysis gas and the decrease of liquid in the experimental yield were attributed to the decomposition of volatile matter during the co-pyrolysis process. At 800 °C, the decrease of char and the increase of liquid in the experimental yield were only observed for BC5-SS5, and the same phenomenon occurred for both BC5-SS5 and BC3-SS7 at 900 °C. The discrepancy of the experimental and theoretical yields of the pyrolysis products of the blends indicated that there were synergistic effects between the BC and SS in the co-pyrolysis process, rather than two independent pyrolysis reaction. The synergistic effects were attributed to the intensified secondary reaction between char and volatile matter, and the more pronounced gas-solid interaction effects, at higher heating rates [25]. The higher H/C molar ratio and the -OH functional groups in SS promoted the formation of a substantial amount of H and OH radicals during pyrolysis. These radicals could serve as hydrogen donors to facilitate the cracking of aromatic compounds in BC and inhibit secondary reactions such as cross-linking, re-condensation and re-polymerisation, thereby increasing the gas yields in the co-pyrolysis process.

In Fig. 4(b), (d) and (f), the primary gas composition generated from the co-pyrolysis of BC and SS consisted of non-condensable gases such as H_2, CH_4, CO, CO_2, and minor amounts of C_2H_2, C_2H_4, C_2H_6. At lower temperatures, the production of H_2 was not only due to the recombination of a major number of H radicals after the cracking of C-H in large molecules, but the water gas shift reactions ($CO + H_2O \rightarrow CO_2 + H_2$, $C + H_2O \rightarrow CO + H_2$) that occurred within the temperature range of 700–900 °C [13]. With the increase in temperature, a substantial amount of CH_4 and a small amount of C_2H_x hydrocarbons were released due to the overlapping cracking reactions of fatty hydrocarbons functional groups and aromatic fatty side chains. The production of CO and CO_2 was associated with the cracking of C=O and -COOH, respectively [26].

When the pyrolysis temperature was constant, as the mass ratio of SS in the blend increased, the yield of H_2 and CH_4 decreased, which was attributed to the larger average molecular structure and higher stability of BC, along with a higher degree of bond cracking and reorganization during condensation reaction [27]. Similarly, under the above conditions, there was a significant increase in the yield of CO_2, while the yields of CO and C_2H_x decreased of 2.62 % and increased of 2.10 %, respectively. This was attributed to that the more of the C in BC was immobilised in the char. At the same mixing ratio, the H_2 yield was proportional to the pyrolysis temperature. This was due to the condensation dehydrogenation reaction between aromatic layers, namely compounds with small number of aromatic rings condensed into higher number of aromatic rings [28], and the catalytic effect of inorganic compounds (ash) on the dehydrogenation reaction during the carbonization process [29]. Concurrently, the CH_4 yield increased and then decreased, while the C_2H_x yield decreased, which was attributed to the different degrees of high-temperature decomposition of volatile matter. The increase in CO yield and decrease in CO_2 yield resulted from that the decarbonylation reaction was prioritised over the decarboxylation reaction at higher temperatures [30].

The experimental yields of H_2, CH_4, and C_2H_x from the co-pyrolysis of BC and SS were higher than the theoretical yields, and there was a maximum increment when the mixing ratio of SS to BC was 7:3, which was 3.09 %, 1.57 %, and 0.99 %, respectively. Meanwhile, there was an obvious decrease in the experimental yields of CO and CO_2. The results indicated that the co-pyrolysis of BC and SS significantly facilitated the yield of high calorific value gaseous hydrocarbons and inhibited the emission of the greenhouse gas as CO_2.

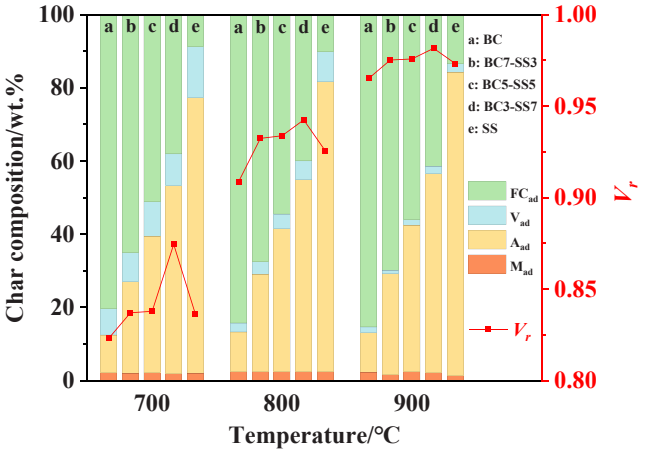

Fig. 5. Rapid co-pyrolysis char composition and volatile matter release rate (V_r) of BC, SS, and blends at 700 ℃, 800 ℃, and 900 ℃.

In addition, according to the proximate analysis results of the raw material and chars of BC, SS and blends, the volatile matter release rate (V_r) could be calculated by Eq. (6):

$$V_r = 1 - \frac{W_{char} \times V_{char}}{W_{raw} \times V_{raw}} \quad (6)$$

where W_{Char} and W_{raw} are the mass (g) of char and raw material, respectively; V_{Char} and V_{raw} are the volatile matter (wt%) of char and raw material, respectively.

The intensity of gas release could be reflected by V_r, and a higher V_r represented a more complete decomposition of volatile matter. In Fig. 5, the V_r of the blends was higher than the individual pyrolysis of BC and SS, and it was proportional to the temperature, indicating that there was a promotion effect on the release of gas products in the co-pyrolysis. The promotion was significant when the mixing ratio of SS to BC was 7:3, as the V_r of BC3-SS7 was the maximum value in the blends at different temperatures, 0.87 at 700°C, 0.94 at 800°C and 0.98 at 900°C.

3.3. FTIR analysis of char samples

The evolution of raw materials and char samples of BC, SS and blends after rapid/slow co-pyrolysis were obtained for the determination of the surface functional groups using FTIR analysis, as shown in Fig. 6, and Table 2 was the band assignments of FTIR spectra. Raw materials exhibited intense absorption peak of -OH at 3700–3000 cm^{-1}, indicating that the -OH content was higher than other functional groups. With the increase of the pyrolysis temperature, the -OH absorption peak in the chars gradually weakened, indicating that the pyrolysis process occurred dehydroxylation reaction, which produced H and OH radicals. The absorption peak did not disappear that was due to the stretching vibration of -OH in the polymers and carboxylic acids still existed. The absorption peak of the C-H at 2923 cm^{-1} and 1450 cm^{-1} were significantly reduced after pyrolysis, which was related to the formation of C_2H_6 and CH_4 by the cracking of -CH_3- and -CH_2, respectively. There was no obvious absorption peak of C=O at 2358 cm^{-1} and C=C at 1656 cm^{-1} in the char, which was related to the susceptible conversion of unstable C=O to CO_2, and the liberation of the high thermal stability C=C as semi-volatile C_2H_4 components. The C≡O, C-C and C-N absorption peak at 1250–850 cm^{-1} indicated the presence of ethers, alcohols, carbon skeletons and amides in BC and SS. Although the strong and broad absorption band of SiO_2 at 1031 cm^{-1} in SS with high ash content might cause some interference in the observation of other functional groups, the absorption peak of the chars in this band have

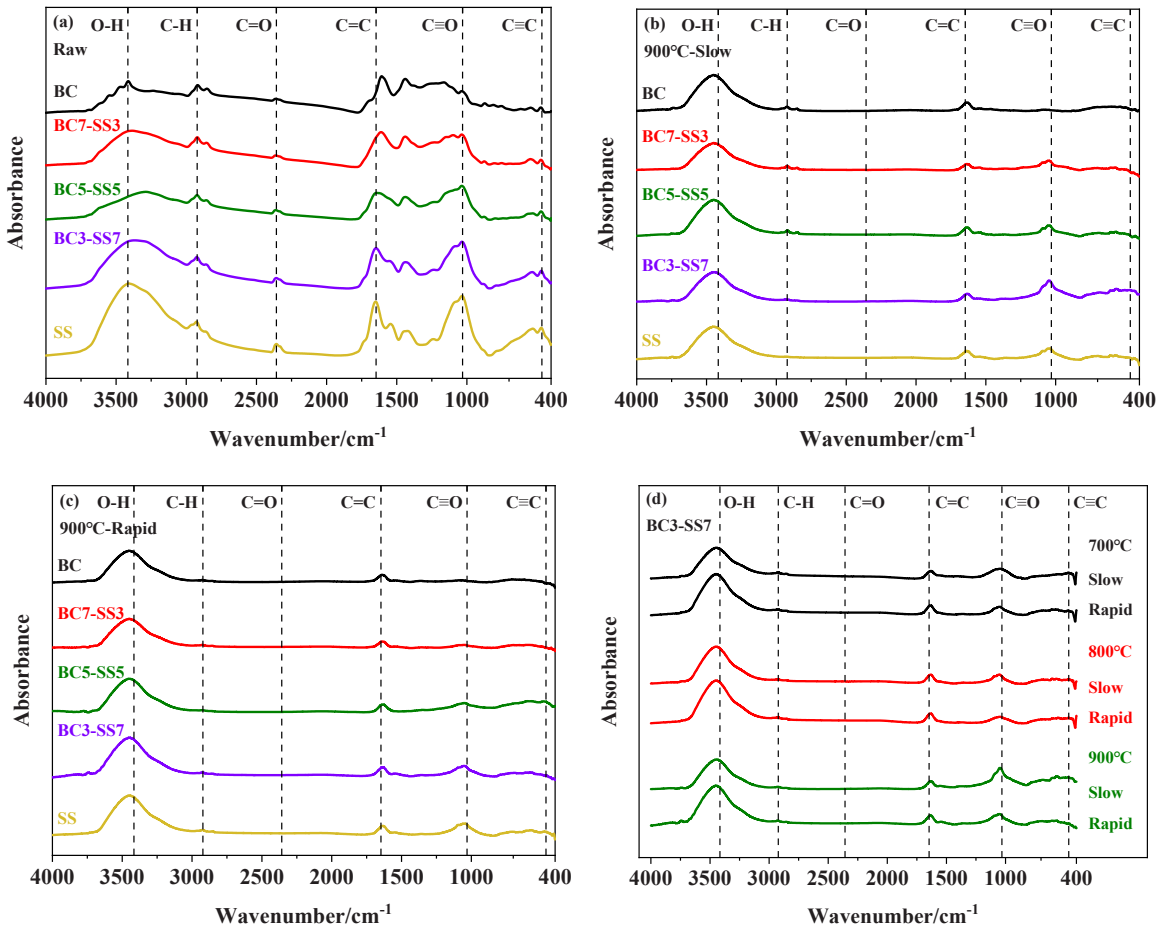

Fig. 6. FTIR spectra of raw material and char of BC, SS, and blends: (a) Raw material, (b) Slow co-pyrolysis char at 900 °C, (c) Rapid co-pyrolysis char at 900 °C, and (d) Rapid/slow co-pyrolysis of BC3-SS7 at 700 °C, 800 °C, and 900 °C.

Table 2
Band assignments of FTIR spectra of raw material and char of BC, SS, and blends [14].

Gas component	Wavenumber/ cm^{-1}	Vibration	Functional group or component
H_2O	3700–3000	Stretching	-OH (hydroxyl or carboxyl group)
C_2H_6	3000–2800	Stretching	-C-H (light alkanes)
CO_2	2400–2250	Stretching	-C=O
C_2H_4	1648	Stretching	C=C (alkenes)
CH_4	1450	Bending	-H-C-H
CO	1250–850	Stretching	-C≡O
C_2H_2, H_2	466	Bending	H-C≡C (alkynes)

already levelled off. This suggested that the C≡O, C-C and C-N have cracked during pyrolysis process, and light oils, small molecules of hydrocarbons, CO and NH_3 have been generated. The changes in the absorption peak at 466 cm^{-1} band were caused by C_2H_2 and H_2 which produced from C≡C cracking in olefinic and aromatic structures.

The characteristic of slow pyrolysis was a lower heating rate, but a longer reaction time; whereas rapid pyrolysis, despite its shorter reaction time, was associated with a higher heating rate. The organic matters in the BC and SS have been decomposed adequately under both pyrolysis conditions. The absorption peak of -OH in the range of 3700–3000 cm^{-1} for the slow pyrolysis chars were attenuated, which was attributed to the more complete release of H_2O over the extended pyrolysis period. On the contrary, the absorption peaks of other functional groups were relatively low during rapid pyrolysis, especially the C≡O absorption peak at 1250–850 cm^{-1} was significantly reduced. These phenomena demonstrated that the rapid temperature increase resulted in a swift release of volatile matter, consequently diminishing the relative abundance of these functional groups. The differences reflected the impact of heating rate on the chemical structure of the materials, slow pyrolysis was more conducive to the retention of certain functional groups, while rapid pyrolysis have resulted in the decrease or disappearance of some functional groups.

3.4. Morphology structure properties of chars

Fig. 7 illustrated the particle morphology and surface structure of the BC, SS, and BC3-SS7 raw materials, and rapid/slow co-pyrolysis chars at 900 °C. For the raw materials, the surface of the BC particle was relatively smooth and dense, without obvious pores and cracks. The SS particle was loose and porous, and the surface was scaly and arranged in a stepped pattern. In the BC3-SS7, there were blocky BC particles with relatively granular SS particles attached. After pyrolysis at 900 °C, some pores and a large number of small particle sediments were formed on the surface of char particle. This phenomenon was more pronounced during the rapid pyrolysis compared to the slow pyrolysis, particularly for the BC3-SS7, which exhibited significant evolution in the pore structure and there was more residual carbon on its surface. The morphological evolution of char particles could be attributed to that, as the pyrolysis temperature increased, the fine particles adhering to the surface were gradually stripped away and the rapid release of volatile matter exposed the sealed pores beneath the surface [31]. In addition, there were significant differences in the surface morphology and microstructure of

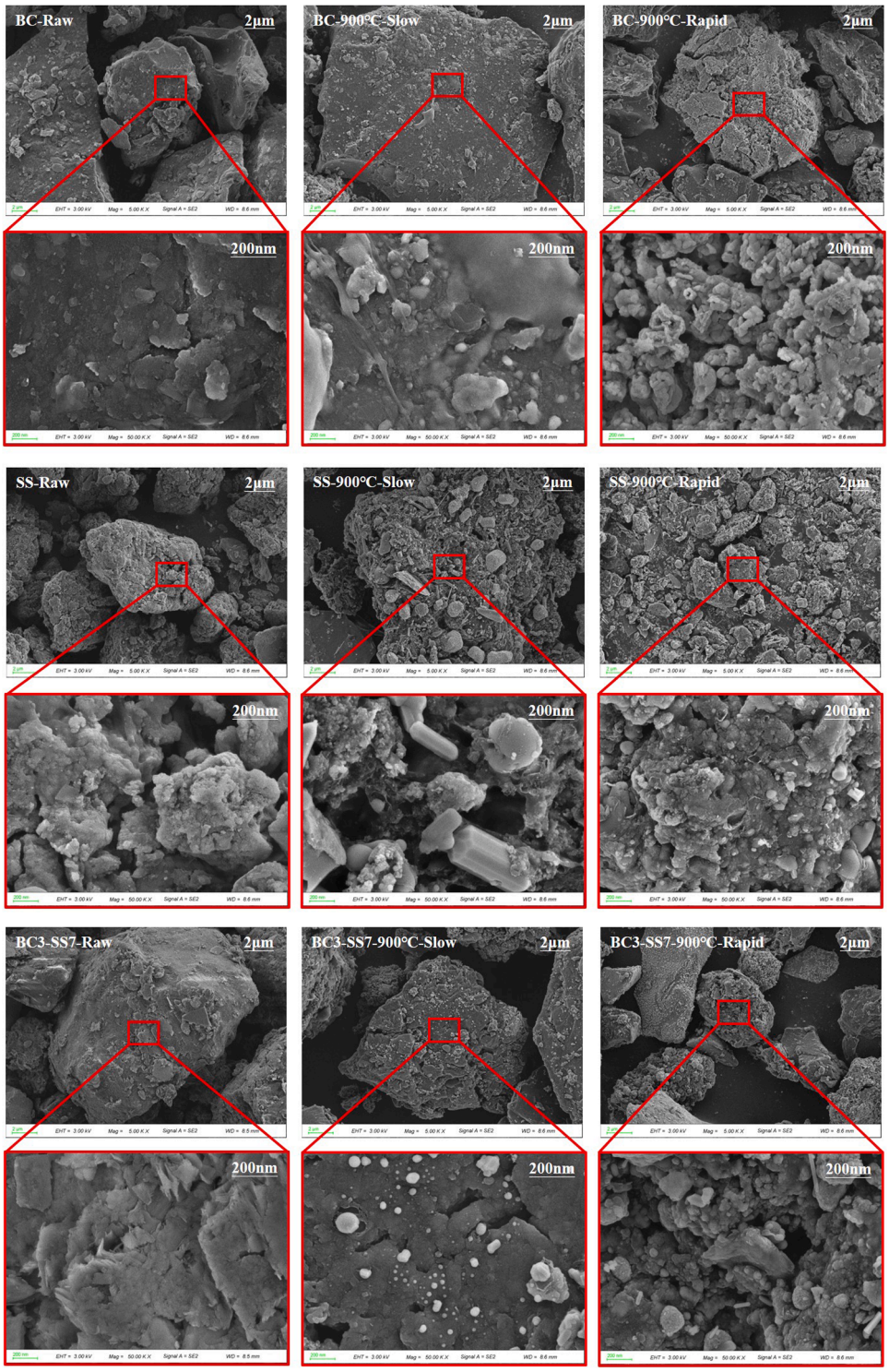

Fig. 7. SEM images of raw material and rapid/slow co-pyrolysis chars of BC, SS, and BC3-SS7 at 900 °C.

chars formed by BC, SS and blends under different pyrolysis conditions. Under the slow pyrolysis condition, the surface of char particles was relatively smooth and partially flocculent, with obvious melting phenomena, indicating that the slow pyrolysis was conducive to the uniform growth of particles and the formation of regular shapes. Under the rapid pyrolysis condition, the structure of the chars was obviously ruptured, and more deposits were formed on the surface of the particles, which indicated that the rapid pyrolysis caused the irregular morphology and denser distribution of the particles, which resulted in the formation of more microscopic pores.

The pore structure parameters of the BC, SS and blends were tested by BET and the results were given in Fig. 8. From Fig. 8(a) - (c), the specific surface area (S_{total}), pore volume (V_{total}), and average pore diameter (D_{avg}) of the raw material and char samples increased with the addition of SS in the mixtures, compared to the raw materials. All these three parameters under the rapid pyrolysis were higher than the results of the slow pyrolysis condition. However, the increments of the specific surface area for the blend sample were 216.8 % and 285.1 % for rapid

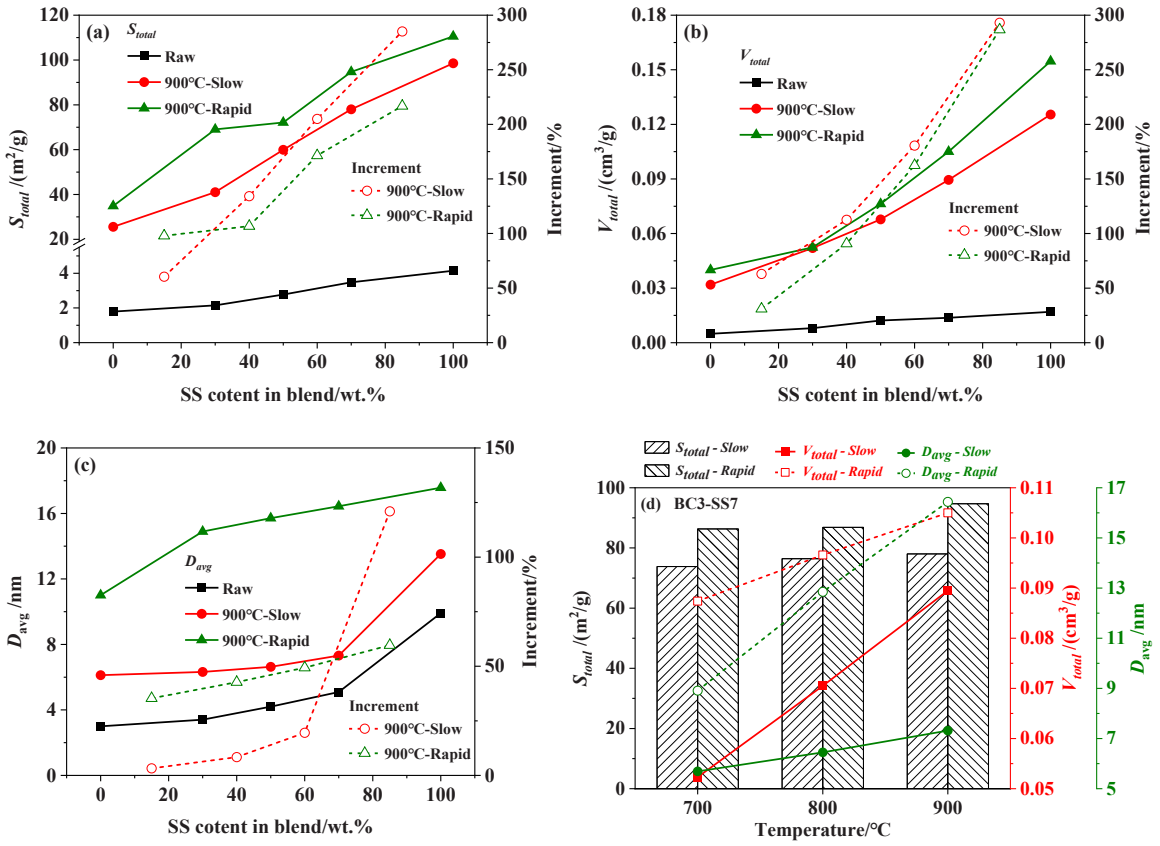

Fig. 8. Micro structure parameters of the raw material and char samples after rapid/slow co-pyrolysis of BC, SS, and blends: (a) S_{total}, (b) V_{total}, (c) D_{avg}, and (d) BC3-SS7.

and slow pyrolysis with adding SS from 0 % to 100 % in the blend in Fig. 8(a). The larger specific surface area was typically corresponded to the smaller particle size or the higher porosity [32]. Similarly, the increments of the V_{total} and D_{avg} were 286.8 % and 59.7 % for rapid pyrolysis and 293.1 % and 120.95 % for slow pyrolysis, which are shown in Fig. 8(b) and (c). In addition, from Fig. 8(d), the with the increasing temperature, the specific surface area for the char sample with a mixing BC/SS ratio of 3:7 in the rapid pyrolysis condition was higher than the value of the slow pyrolysis condition. Both V_{total} and D_{avg} increased with the pyrolysis temperature and the rapid pyrolysis condition yielded higher values. The volatile matter releasing caused the extension of pores such as micropores and mesopores, which further enlarge the pore volume and size during pyrolysis [33]. This phenomenon was also associated with the increase mixing ratio of SS, with a higher volatile content, tended to form mesopores during pyrolysis, whereas the BC formed a large number of micropores with the decomposition of fixed carbon [34].

In Fig. 9(a), the particle size of the raw materials was ranged from 133 to 146 μm. After the pyrolysis of the BC, SS and blends, the overall particle size distribution region of chars was concentrated from the 1–200 μm to the 10–100 μm with a slight decrease in particle size. This was attributed to that under high temperature and rapid pyrolysis conditions, the larger particles released more volatile matter and broke up to form smaller particles, while the smaller particles softened and deformed, and partially melted with each other to form larger particles. In the pyrolysis reaction, as the particle size increased, the reactivity of the char would be inhibited due to the enhanced diffusion limitation [35]. If the pyrolysis was carried out with particles smaller than 270 μm, the optimum combined pyrolysis property index and weight loss rate could be achieved [36]. There was no significant change in particle size before and after pyrolysis under different conditions, indicating that the increase in the surface area of char was primarily attributed to its more developed porous structure.

3.5. Pyrolysis kinetic analyses

In this study, the co-pyrolysis kinetic parameters of BC and SS were calculated from the TG data, which were obtained under non-isothermal and heterogeneous conditions, and the kinetic equation of the co-pyrolysis reaction. When c (concentration) was replaced by α (thermal conversion) in the isothermal and homogeneous reaction kinetic equation, the non-isothermal process was divided into innumerable isothermal stages.

$$\frac{d\alpha}{dt} = k(T)f(\alpha) \tag{7}$$

where α is the thermal conversion (%) at time t (min); $d\alpha/dt$ is the decomposition rate (%/min); $k(T)$ is the rate constant expressed by the Arrhenius equation; $f(\alpha)$ is the kinetic model;

$$\alpha = \frac{m_i - m_t}{m_i - m_f} \tag{8}$$

$$f(\alpha) = (1-\alpha)^n \tag{9}$$

$$k(T) = A \cdot \exp\left(-\frac{E}{RT}\right) \tag{10}$$

where m_i, m_t and m_f refers to the initial, instantaneous and final weight (g), respectively; n represents the reaction order of the co-pyrolysis kinetic model; A and E are the pre-exponential factor (min^{-1}) and activation energy (kJ/mol), respectively; R and T are the universal gas constant (J/(mol K)) and absolute temperature (K), respectively;

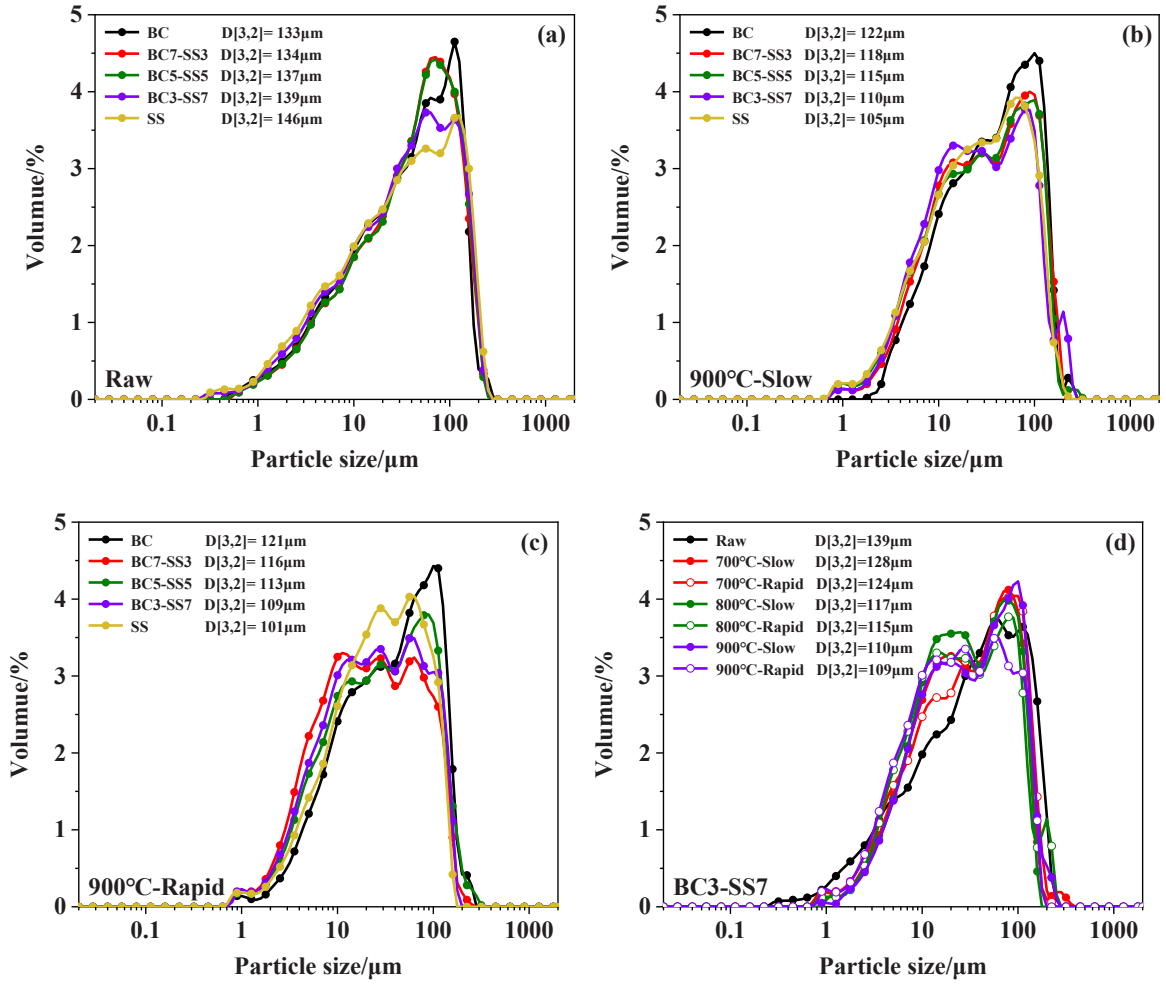

Fig. 9. Particle size distribution of raw material and char of BC, SS, and blends: (a) Raw, (b) Slow co-pyrolysis at 900 ℃, (c) Rapid co-pyrolysis at 900 ℃, and (d) Rapid/slow co-pyrolysis of BC3-SS7 at 700 °C, 800 °C, and 900 °C.

combining and rearranging Eqs. (8–10) to Eq. (11):

$$\frac{d\alpha}{dt} = A\cdot\exp\left(-\frac{E}{RT}\right)\left(1-\frac{m_i-m_t}{m_i-m_f}\right)^n \tag{11}$$

adopting a fixed heating rate β (10 K/min) as Eq. (12), and bringing it into Eq. (11) while taking the natural logarithm on both sides as Eq. (13):

$$\beta = \frac{dT}{dt} \tag{12}$$

$$\ln\frac{d\alpha/dT}{(1-\alpha)^n} = \ln\frac{A}{\beta} - \frac{E}{RT} \tag{13}$$

the straight line of $\ln[(d\alpha/dT)/(1-\alpha)^n]$ versus $1/T$ is obtained as Eq. (13); the pre-exponential factor A and the activation energy E can be calculated from the slope and intercept of this straight line, respectively.

According to the slow co-pyrolysis data, the DTG curves of the S-II stage in Fig. 2(b) were differentiated once to segment the temperature stages based on the monotonically increasing or decreasing regions before and after the peak [37]. The individual pyrolysis peak of BC and SS was at the S-II-II and S-II-I, respectively, which could be divided into two temperature stages. The co-pyrolysis of BC and SS had one peak in both S-II-I and S-II-II, which could be divided into four temperature stages: L-I (453–573 K), L-II (573–653 K), H-I (653–723 K) and H-II (723–843 K). The co-pyrolysis of BC and SS was a complex physico-chemical reaction process, the relevance of the $f(\alpha)$ could not be ensured if a single n was used for kinetic calculation. Therefore, the data was taken at intervals of 10 K in TG, and using different n (0.1, 0.2, 0.3, 0.5, 0.75, 1.0, 1.5, 2.0, 3.0) for linear fitting trials to determine the optimal correlation coefficient (R^2). The mass average activation energy (E_m) [38] was introduced due to E could not indicate the e entire reaction volution, where F represents the weight loss in each temperature stage as Eq. (14):

$$E_m = E_1\times F_1 + E_2\times F_2 + \ldots + E_n\times F_n \tag{14}$$

The kinetic fitting curves were presented in Fig. 10, and the optimal $f(\alpha)$ and its corresponding kinetic parameters were shown in Table 3. The optimal n corresponding to each stage of the co-pyrolysis reaction was the same as that of BC (n=0.75) in the S-II-II stage and that of SS (n=2, 0.2) in the S-II-I stage. Each of the R^2 value were fallen within the range of 0.9822–0.9980, indicating a high degree of reliability for these results.

The E_m of the co-pyrolysis reaction were as follows: BC7-SS3: 11.92 kJ/mol, BC5-SS5: 10.70 kJ/mol, BC3-SS7: 10.32 kJ/mol, all of which were less than the E_m of the individual pyrolysis of BC (21.16 kJ/mol) and SS (12.34 kJ/mol). The least E_m was observed when the mass ratio of SS was 70 %, indicating that the energy required for co-pyrolysis was the minimum at this composition. Furthermore, as the mass ratio of BC increased from 30 % to 70 %, the E_m in the co-pyrolysis process correspondingly augmented. This phenomenon was associated with the volatile content composition of BC, suggesting that a higher energy was required for the co-pyrolysis of heavier volatile matter and char [39].

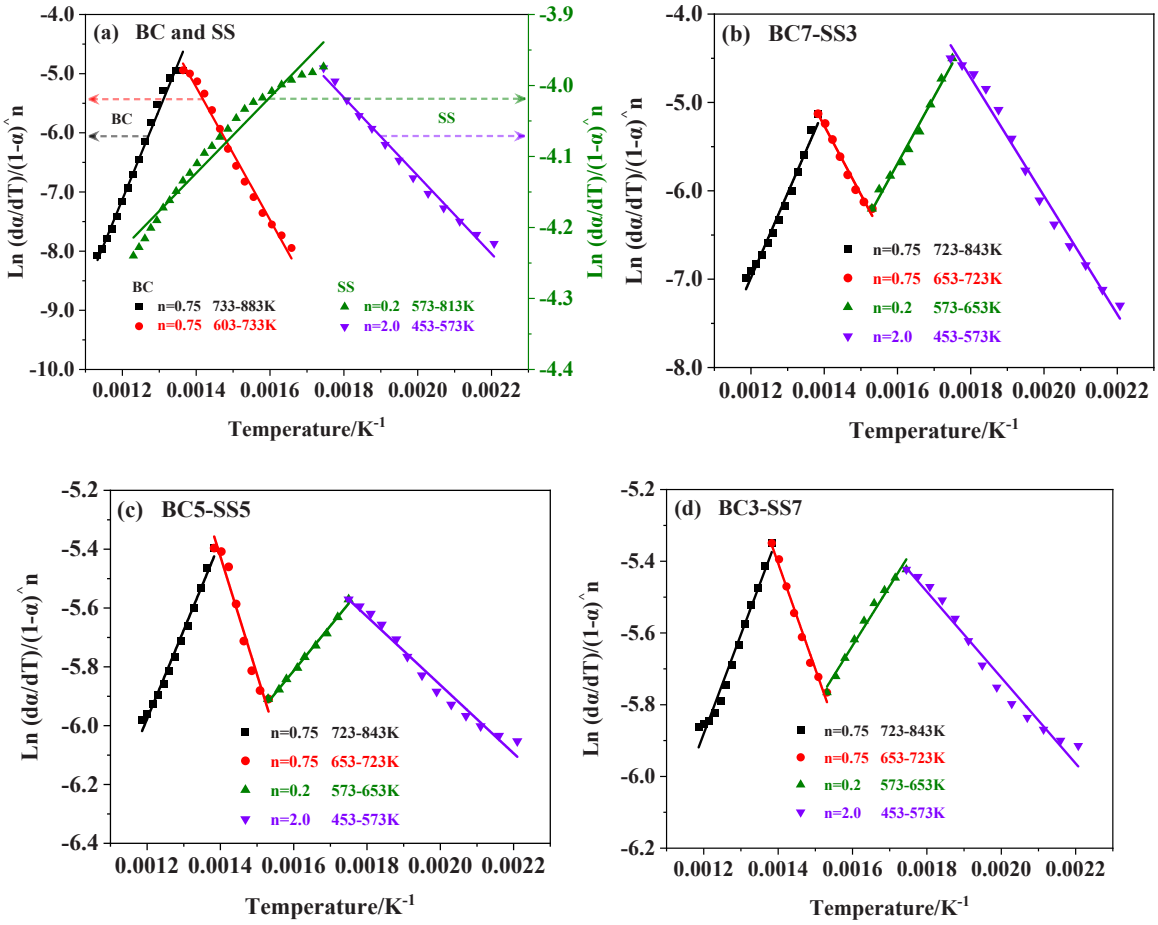

Fig. 10. Kinetic fitting curves of BC, SS, and blends in different reaction orders and temperature ranges: (a) BC and SS, (b) BC7-SS3, (c) BC5-SS5, and (d) BC3-SS7.

Table 3
Kinetic parameters of co-pyrolysis of BC, SS, and blends.

Material	Region/K	E/kJ mol^{-1}	A/min^{-1}	$f(\alpha)$	R^2	F/wt%	E_m/kJ mol^{-1}
BC	603–733	93.23	3.522×10^{5}	$(1-\alpha)^{0.75}$	0.9890	7.79	21.16
	733–883	51.47	1.118×10^{-3}	$(1-\alpha)^{0.75}$	0.9890	9.87	
SS	453–573	42.88	4.850×10^{-1}	$(1-\alpha)^{2}$	0.9891	12.62	12.34
	573–813	72.93	3.710×10^{-3}	$(1-\alpha)^{0.2}$	0.9840	25.05	
BC7-SS3	453–573	55.64	3.651×10^{3}	$(1-\alpha)^{2}$	0.9879	3.54	11.92
	573–653	13.04	5.203×10^{-3}	$(1-\alpha)^{0.2}$	0.9895	4.60	
	653–723	64.72	2.801×10^{3}	$(1-\alpha)^{0.75}$	0.9860	5.70	
	723–843	50.54	7.725×10^{-4}	$(1-\alpha)^{0.75}$	0.9906	8.04	
BC5-SS5	453–573	49.77	1.064×10^{3}	$(1-\alpha)^{2}$	0.9893	6.39	10.70
	573–653	23.03	2.587×10^{-3}	$(1-\alpha)^{0.2}$	0.9980	7.19	
	653–723	38.38	2.982×10^{1}	$(1-\alpha)^{0.75}$	0.9837	6.04	
	723–843	50.51	6.784×10^{-4}	$(1-\alpha)^{0.75}$	0.9893	7.31	
BC3-SS7	453–573	47.80	2.157×10^{3}	$(1-\alpha)^{2}$	0.9844	8.88	10.32
	573–653	27.65	1.961×10^{-3}	$(1-\alpha)^{0.2}$	0.9822	9.50	
	653–723	24.52	2.789×10^{0}	$(1-\alpha)^{0.75}$	0.9870	6.50	
	723–843	50.18	5.666×10^{-4}	$(1-\alpha)^{0.75}$	0.9909	6.49	

Within the L-I stage, where the weight loss rate gradually increased, the E of BC7-SS3, BC5-SS5, BC3-SS7, and SS was inversely proportional to the mass ratio of SS in the blends, which was 55.64 kJ/mol, 49.77 kJ/mol, 47.80 kJ/mol and 42.88 kJ/mol, respectively. The weight loss of BC within the whole S-II-I stage was only 4.31 wt%, which was much less than the conversion rate of the blends, indicating that the variation of E in this stage was primarily influenced by SS. Similarly, within the H-II stage, the E of the co-pyrolysis process was proportional to the mass ratio of BC in the blends and its average difference was only 0.43 kJ/mol, which was related to the closer conversion of the blends [40]. In summary, during the co-pyrolysis process, both the E for a specific stage and the E_m for the entire reaction were lower than the individual pyrolysis of BC and SS, suggesting that there were significant positive synergistic effects in the co-pyrolysis process [41]. The mutual promotion between the BC and SS not only markedly reduced the activation energy required for the pyrolysis reaction of the blends, but improved the comprehensive pyrolysis characteristics index.

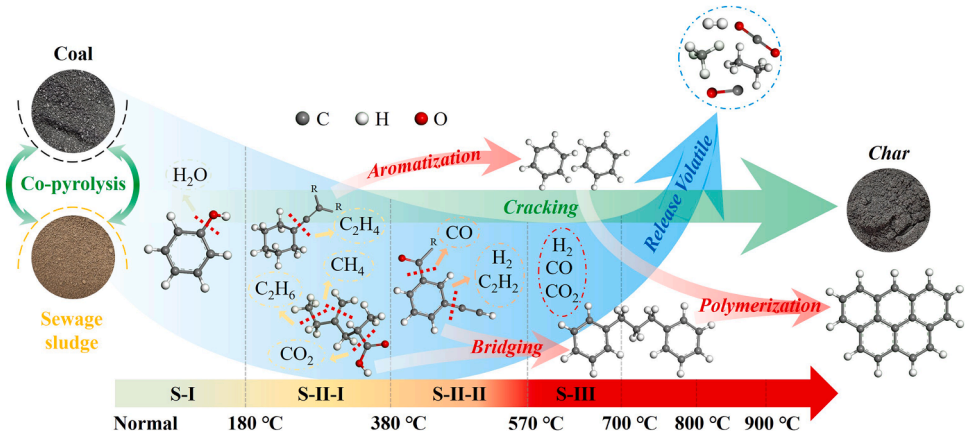

Fig. 11. Schematic diagram of the co-pyrolysis synergistic mechanism of the BC and SS mixtures under rapid/slow heating conditions.

3.6. Co-pyrolysis synergistic mechanisms

To clarify the product release characteristics and interactions in the co-pyrolysis of the BC and SS, according to the experimental results above, the schematic diagram of the co-pyrolysis synergistic mechanism of the BC and SS mixtures under rapid/slow heating conditions was proposed in Fig. 11. For the slow co-pyrolysis, the cleavage of long chain alkane and double bonded alkene in the BC and SS resulted in the production of a significant number of hydrogen radicals, which combined with other functional groups and continued to participate in the subsequent pyrolysis. Dehydroxylation reaction occurred in the low temperature of S-I stage. At the S-II-I stage, the five membered ring aliphatic hydrocarbon side chains were cleaved to release C_2H_4. The chain hydrocarbon side chain functional groups were broken while releasing C_2H_6, and due to the SS was decomposed earlier than the BC, majority of the CH_4 generated from the demethylation reaction and the CO_2 formed from the decarboxylation reaction were from the SS. As the temperature rose to the S-II-II stage, the aromatic hydrocarbon side chains in the BC and SS were cleaved to form hydrocarbon and oxygenated radicals, releasing H_2, C_2H_2 and CO. Entering the S-III stage, gas products such as H_2, CO, and CO_2 continued to be released. Five membered ring formed benzene ring through aromatization cyclization reaction, the short aliphatic chains formed bridges between the small aromatic rings owing to the high activity, and could form alkyl-linked biphenyl compounds. The alkyl-linked biphenyl structure could polymerise to polycyclic aromatic hydrocarbons as benzene, phenanthrene and benzopyrene. Although the reaction time in the rapid co-pyrolysis was relatively short, the higher heating conditions would cause intense cleavage of molecular compound and a higher degree of aromatization polymerization and cycloaddition reaction in the BC and SS, and the small ring aromatics aggregated to form large ring aromatics. The rapid co-pyrolysis would swiftly pass through the medium and low temperature stages and release volatile components, and upon reaching the high temperature stage, the semi-coke progressively converted into char.

4. Conclusion

In this study, the co-pyrolysis characteristics and synergistic mechanism of sewage sludge and low rank coal were investigated under rapid/slow heating conditions with experimental and analytical methods. Under the slow heating condition, the CO_2 was released before 380 °C. As the temperature rose, gases such as CO, CH_4, C_2H_2, C_2H_4 and C_2H_6 were progressively liberated, and H_2 was generated at higher temperatures (≥570 ℃). During the rapid co-pyrolysis, the long aliphatic chain cyclised and aromatised, the small aromatic ring bound to the short aliphatic chain and bridged to biphenyl structure, which polymerized to the larger aromatic ring system as the volatile components were released. When the mass ratio of sludge in the blend was 70 %, the experimental and theoretical yields of char was essentially equivalent, whereas the yield of gas products could be increased by 2.30 %, with the majority of this increment being high value combustible gases. The blend at this mixing ratio also had the minimum E_m as 10.32 kJ/mol, which was lower than that of BC7-SS3 (11.92 kJ/mol) and BC5-SS5 (10.70 kJ/mol). The large amount of volatile matter in SS promoted the co-pyrolysis reaction, there was a positive synergistic effect of co-pyrolysis of BC and SS, which was significant when the reactants were BC3-SS7, and especially facilitated the yield of high calorific value gaseous hydrocarbons. This study elucidated the synergistic pyrolysis characteristics and reaction mechanisms of sewage sludge and low rank coal, which would establish a foundation for the efficient utilization of sewage sludge and low rank coal through co-pyrolysis.

CRediT authorship contribution statement

Chenyang Liu: Writing – review & editing, Writing – original draft, Visualization, Validation, Software, Resources, Methodology, Investigation, Formal analysis, Data curation, Conceptualization. **Zhongjie Shen:** Writing – review & editing, Supervision, Project administration, Funding acquisition, Conceptualization. **Haigang Zhang:** Validation, Resources, Methodology, Formal analysis. **Guinan He:** Software, Methodology, Formal analysis. **Weifeng Li:** Supervision, Project administration, Funding acquisition. **Haifeng Liu:** Supervision, Project administration, Funding acquisition.

Declaration of Competing Interest

The authors declare that they have no known competing financial interests or personal relationships that could have appeared to influence the work reported in this paper.

Acknowledgements

This study is supported by the National Key Research and Development Program of China (2022YFC3902502-04), National Natural Science Foundation of China (22378130), Fundamental Research Funds of the Central Universities (2022ZFJH004).

Appendix A. Supporting information

Supplementary data associated with this article can be found in the online version at doi:10.1016/j.jaap.2024.106873.

Data Availability

The authors are unable or have chosen not to specify which data has been used.

References

[1] S.R. Naqvi, I. Ali, S. Nasir, S. Ali Ammar Taqvi, A.E. Atabani, W.-H. Chen, Assessment of agro-industrial residues for bioenergy potential by investigating thermo-kinetic behavior in a slow pyrolysis process, Fuel 278 (2020), https://doi.org/10.1016/j.fuel.2020.118259.

[2] G. Jiang, D. Xu, B. Hao, L. Liu, S. Wang, Z. Wu, Thermochemical methods for the treatment of municipal sludge, J. Clean. Prod. 311 (2021), https://doi.org/10.1016/j.jclepro.2021.127811.

[3] P. Ling, D. Chen, K. Xu, J. Xu, M.E. Mostafa, L. Jiang, Y. Wang, S. Su, S. Hu, J. Xiang, Insight into the synergistic effect on thermal behavior in co-pyrolysis of coal slime and sewage sludge: kinetics, thermodynamics, dendrite neural network modelling, and evolved char structure, J. Clean. Prod. 450 (2024), https://doi.org/10.1016/j.jclepro.2024.141790.

[4] T. Wang, Y. Chen, J. Li, Y. Xue, J. Liu, M. Mei, H. Hou, S. Chen, Co-pyrolysis behavior of sewage sludge and rice husk by TG-MS and residue analysis, J. Clean. Prod. 250 (2020), https://doi.org/10.1016/j.jclepro.2019.119557.

[5] L. Zheng, Z. Liu, J. Jin, X. He, B. Liu, Mechanisms for NO_x emission control and ash deposition mitigation in sludge-coal blend combustion, J. Clean. Prod. 455 (2024), https://doi.org/10.1016/j.jclepro.2024.142284.

[6] J. Jin, Y. Li, J. Zhang, S. Wu, Y. Cao, P. Liang, J. Zhang, M.H. Wong, M. Wang, S. Shan, P. Christie, Influence of pyrolysis temperature on properties and environmental safety of heavy metals in biochars derived from municipal sewage sludge, J. Hazard. Mater. 320 (2016) 417, https://doi.org/10.1016/j.jhazmat.2016.08.050.

[7] S.S.A. Syed-Hassan, Y. Wang, S. Hu, S. Su, J. Xiang, Thermochemical processing of sewage sludge to energy and fuel: fundamentals, challenges and considerations, Renew. Sust. Energ. Rev. 80 (2017) 888, https://doi.org/10.1016/j.rser.2017.05.262.

[8] Q. Zhang, H. Liu, P. Liu, H. Hu, H. Yao, Pyrolysis characteristics and kinetic analysis of different dewatered sludge, Bioresour. Technol. 170 (2014) 325, https://doi.org/10.1016/j.biortech.2014.07.111.

[9] J. Shao, R. Yan, H. Chen, H. Yang, D.H. Lee, Catalytic effect of metal oxides on pyrolysis of sewage sludge, Fuel Process. Technol. 91 (2010) 1113, https://doi.org/10.1016/j.fuproc.2010.03.023.

[10] A. Magdziarz, S. Werle, Analysis of the combustion and pyrolysis of dried sewage sludge by TGA and MS, Waste Manag. 34 (2014) 174, https://doi.org/10.1016/j.wasman.2013.10.033.

[11] L. Han, J. Li, C. Qu, Z. Shao, T. Yu, B. Yang, Recent progress in sludge co-pyrolysis technology, Sustainability 14 (2022), https://doi.org/10.3390/su14137574.

[12] Z. Hameed, S.R. Naqvi, M. Naqvi, I. Ali, S.A.A. Taqvi, N. Gao, S.A. Hussain, S. Hussain, A comprehensive review on thermal coconversion of biomass, sludge, coal, and their blends using thermogravimetric analysis, J. Chem. 2020 (2020) 1, https://doi.org/10.1155/2020/5024369.

[13] L. Mu, J. Chen, P. Yao, D. Zhou, L. Zhao, H. Yin, Evaluation of co-pyrolysis petrochemical wastewater sludge with lignite in a thermogravimetric analyzer and a packed-bed reactor: Pyrolysis characteristics, kinetics, and products analysis, Bioresour. Technol. 221 (2016) 147, https://doi.org/10.1016/j.biortech.2016.09.011.

[14] C. He, C. Tang, W. Liu, L. Dai, R. Qiu, Co-pyrolysis of sewage sludge and hydrochar with coals: Pyrolytic behaviors and kinetics analysis using TG-FTIR and a discrete distributed activation energy model, Energy Convers. Manag. 203 (2020), https://doi.org/10.1016/j.enconman.2019.112226.

[15] B. Zhao, J. Jin, S. Li, D. Liu, R. Zhang, H. Yang, Co-pyrolysis characteristics of sludge mixed with Zhundong coal and sulphur contaminant release regularity, J. Therm. Anal. Calorim. 138 (2019) 1623, https://doi.org/10.1007/s10973-019-08300-x.

[16] N. Gao, J. Li, C. Quan, H. Tan, Product property and environmental risk assessment of heavy metals during pyrolysis of oily sludge with fly ash additive, Fuel 266 (2020), https://doi.org/10.1016/j.fuel.2020.117090.

[17] R.N. Coimbra, S. Paniagua, C. Escapa, L.F. Calvo, M. Otero, Thermogravimetric analysis of the co-pyrolysis of a bituminous coal and pulp mill sludge, J. Therm. Anal. Calorim. 122 (2015) 1385, https://doi.org/10.1007/s10973-015-4834-3.

[18] R.N. Coimbra, S. Paniagua, C. Escapa, L.F. Calvo, M. Otero, Thermal Valorization of Pulp Mill Sludge by Co-processing with Coal, Waste Biomass-.-. Valoriz. 7 (2016) 995, https://doi.org/10.1007/s12649-016-9524-2.

[19] S. Fang, Z. Yu, Y. Lin, Y. Lin, Y. Fan, Y. Liao, X. Ma, A study on experimental characteristic of co-pyrolysis of municipal solid waste and paper mill sludge with additives, Appl. Therm. Eng. 111 (2017) 292, https://doi.org/10.1016/j.applthermaleng.2016.09.102.

[20] S. Deng, H. Tan, X. Wang, F. Yang, R. Cao, Z. Wang, R. Ruan, Investigation on the fast co-pyrolysis of sewage sludge with biomass and the combustion reactivity of residual char, Bioresour. Technol. 239 (2017) 302, https://doi.org/10.1016/j.biortech.2017.04.067.

[21] Y. Song, A. Tahmasebi, J. Yu, Co-pyrolysis of pine sawdust and lignite in a thermogravimetric analyzer and a fixed-bed reactor, Bioresour. Technol. 174 (2014) 204, https://doi.org/10.1016/j.biortech.2014.10.027.

[22] Z. Wang, X. Ma, Z. Yao, Q. Yu, Z. Wang, Y. Lin, Study of the pyrolysis of municipal sludge in N_2/CO_2 atmosphere, Appl. Therm. Eng. 128 (2018) 662, https://doi.org/10.1016/j.applthermaleng.2017.09.044.

[23] H. Song, G. Liu, J. Zhang, J. Wu, Pyrolysis characteristics and kinetics of low rank coals by TG-FTIR method, Fuel Process. Technol. 156 (2017) 454, https://doi.org/10.1016/j.fuproc.2016.10.008.

[24] M.B. Folgueras, R.M. Díaz, J. Xiberta, Pyrolysis of blends of different types of sewage sludge with one bituminous coal, Energy 30 (2005) 1079, https://doi.org/10.1016/j.energy.2004.08.001.

[25] Z. Zhu, Y. Huang, M. Yu, J. Gao, H. Cheng, Z. Li, W. Xu, Y. Xiao, Co-combustion of bituminous coal and industrious sludge under non-isothermal and isothermal conditions: Thermal behaviors, kinetic analyses, and heavy metals migration, J. Clean. Prod. 434 (2024), https://doi.org/10.1016/j.jclepro.2023.140167.

[26] J. Liu, X. Jiang, J. Shen, H. Zhang, Pyrolysis of superfine pulverized coal. Part 2. Mechanisms of carbon monoxide formation, Energy Convers. Manag. 87 (2014) 1039, https://doi.org/10.1016/j.enconman.2014.07.055.

[27] K. Zhang, P. Lu, X. Guo, L. Wang, H. Lv, Z. Wang, Y. He, High-temperature pyrolysis behavior of two different rank coals in fixed-bed and drop tube furnace reactors, J. Energy Inst. 93 (2020) 2271, https://doi.org/10.1016/j.joei.2020.06.010.

[28] M. Wang, Z. Li, W. Huang, J. Yang, H. Xue, Coal pyrolysis characteristics by TG–MS and its late gas generation potential, Fuel 156 (2015) 243, https://doi.org/10.1016/j.fuel.2015.04.055.

[29] I. Fonts, M. Azuara, G. Gea, M.B. Murillo, Study of the pyrolysis liquids obtained from different sewage sludge, J. Anal. Appl. Pyrolysis 85 (2009) 184, https://doi.org/10.1016/j.jaap.2008.11.003.

[30] J. Alvarez, M. Amutio, G. Lopez, I. Barbarias, J. Bilbao, M. Olazar, Sewage sludge valorization by flash pyrolysis in a conical spouted bed reactor, Chem. Eng. J. 273 (2015) 173, https://doi.org/10.1016/j.cej.2015.03.047.

[31] W. Xia, C. Niu, C. Ren, Enhancement in floatability of sub-bituminous coal by low-temperature pyrolysis and its potential application in coal cleaning, J. Clean. Prod. 168 (2017) 1032, https://doi.org/10.1016/j.jclepro.2017.09.119.

[32] K. Zhang, Y. Li, Y. He, Z. Wang, Q. Li, M. Kuang, L. Ge, K. Cen, Volatile gas release characteristics of three typical Chinese coals under various pyrolysis conditions, J. Energy Inst. 91 (2018) 1045, https://doi.org/10.1016/j.joei.2017.07.004.

[33] J. Xiao, F. Li, Q. Zhong, J. Huang, B. Wang, Y. Zhang, Effect of high-temperature pyrolysis on the structure and properties of coal and petroleum coke, J. Anal. Appl. Pyrolysis 117 (2016) 64, https://doi.org/10.1016/j.jaap.2015.12.015.

[34] A. Méndez, M. Terradillos, G. Gascó, Physicochemical and agronomic properties of biochar from sewage sludge pyrolysed at different temperatures, J. Anal. Appl. Pyrolysis 102 (2013) 124, https://doi.org/10.1016/j.jaap.2013.03.006.

[35] C. Guizani, F.J.E. Sanz, S. Salvador, Influence of temperature and particle size on the single and mixed atmosphere gasification of biomass char with H_2O and CO_2, Fuel Process. Technol. 134 (2015) 175. ⟨https://hal.science/hal-01662704⟩.

[36] Y. Li, X. Xing, B. Xu, Y. Xing, X. Zhang, J. Yang, J. Xing, Effect of the particle size on co-cOmbustion of Municipal Solid Waste and Biomass Briquette under N_2/O_2 and CO_2/O_2 atmospheres, Energy Fuels 31 (2016) 932, https://doi.org/10.1021/acs.energyfuels.6b02705.

[37] M.B. Folgueras, R.M. Díaz, J. Xiberta, I. Prieto, Thermogravimetric analysis of the co-combustion of coal and sewage sludge, Fuel 82 (2003) 2051, https://doi.org/10.1016/s0016-2361(03)00161-3.

[38] C. W, Reactivity assessment of coals via a weighted mean activation energy, Fuel 63 (1984) 1436, https://doi.org/10.1016/0016-2361(84)90353-3.

[39] X. Zhuang, Y. Song, H. Zhan, X. Yin, C. Wu, Synergistic effects on the co-combustion of medicinal biowastes with coals of different ranks, Renew. Energy 140 (2019) 380, https://doi.org/10.1016/j.renene.2019.03.070.

[40] Z. Wu, S. Wang, J. Zhao, L. Chen, H. Meng, Synergistic effect on thermal behavior during co-pyrolysis of lignocellulosic biomass model components blend with bituminous coal, Bioresour. Technol. 169 (2014) 220, https://doi.org/10.1016/j.biortech.2014.06.105.

[41] Z. Wu, J. Zhang, Y. Fan, B. Zhang, W. Guo, R. Zhang, Y. Li, B. Yang, Synergistic effects from co-pyrolysis of lignocellulosic biomass with low-rank coal: a perspective based on the interaction of organic components, Fuel 306 (2021), https://doi.org/10.1016/j.fuel.2021.121648.